Energy Engineering

Tech Science Press

DOI: 10.32604/ee.2023.043082

ARTICLE

An Adaptive Control Strategy for Energy Storage Interface Converter Based on Analogous Virtual Synchronous Generator

Feng Zhao, Jinshuo Zhang*, Xiaoqiang Chen and Ying Wang

School of Automation and Electrical Engineering, Lanzhou Jiaotong University, Lanzhou, 730070, China

*Corresponding Author: Jinshuo Zhang. Email: jinshuozhang2022@163.com

Received: 26 June 2023 Accepted: 14 September 2023 Published: 25 January 2024

ABSTRACT

In the DC microgrid, the lack of inertia and damping in power electronic converters results in poor stability of DC bus voltage and low inertia of the DC microgrid during fluctuations in load and photovoltaic power. To address this issue, the application of a virtual synchronous generator (VSG) in grid-connected inverters control is referenced and proposes a control strategy called the analogous virtual synchronous generator (AVSG) control strategy for the interface DC/DC converter of the battery in the microgrid. Besides, a flexible parameter adaptive control method is introduced to further enhance the inertial behavior of the AVSG control. Firstly, a theoretical analysis is conducted on the various components of the DC microgrid, the structure of analogous virtual synchronous generator, and the control structure's main parameters related to the DC microgrid's inertial behavior. Secondly, the voltage change rate tracking coefficient is introduced to adjust the change of the virtual capacitance and damping coefficient flexibility, which further strengthens the inertia trend of the DC microgrid. Additionally, a small-signal modeling approach is used to analyze the approximate range of the AVSG's main parameters ensuring system stability. Finally, conduct a simulation analysis by building the model of the DC microgrid system with photovoltaic (PV) and battery energy storage (BES) in MATLAB/Simulink. Simulation results from different scenarios have verified that the AVSG control introduces fixed inertia and damping into the droop control of the battery, resulting in a certain level of inertia enhancement. Furthermore, the additional adaptive control strategy built upon the AVSG control provides better and flexible inertial support for the DC microgrid, further enhances the stability of the DC bus voltage, and has a more positive impact on the battery performance.

KEYWORDS

Adaptive control; analogous virtual synchronous generator; DC/DC converter; inertia of DC microgrid; DC microgrid with PV and BES; battery; DC bus voltage

Nomenclature

J	Moments of inertia
C_v	Virtual capacitance (F)
D_p	Damping coefficient
k_{droop}	Droop coefficient
P_e	Electromagnetic power (W)
P_D	Damping power (W)
P_{set}	The $P-\omega$ droop control output power (W)
P_{pv}	Photovoltaic output power (W)

P_{load}	Load output power (W)
ω	The angular velocity
ω_N	Rated angular velocity
u_{dc}^*	Output voltage of AVSG (V)
u_N	The rated voltage of AVSG (V)
u_{dc}	DC bus voltage (V)
Δi	Virtual capacitance current (A)
i_{set}	The $P-\omega$ droop control input current (A)
i_{dc}	DC bus current (A)
i_{d}	Damping current (A)
S_{pv}	Solar irradiance (W/m^2)
I_{L}	Inductive current of the battery (A)
SOC	State of charge of the battery
A	Voltage change rate tracking coefficient of C_{v}
B	Voltage change rate tracking coefficient of D_{p}

1 Introduction

In recent years, the issues of energy scarcity and environmental pollution have driven a transition in the generation mode of the power system from traditional centralized power generation to distributed power generation [1,2]. As a type of power system, the DC microgrid has gained widespread attention due to its suitability for large-scale integration of distributed power sources. And compared with the AC microgrid, the DC microgrid does not need to consider factors such as frequency, reactive power, and phase, resulting in higher power supply quality [3].

In the DC microgrid, the power balance among distributed source, energy storage unit, and load ensures the stability of the DC bus voltage, which serves as a critical indicator for the secure and stable operation of the system. The DC microgrid form adopted in this paper is a photovoltaic (PV) and battery energy storage (BES)-integrated DC microgrid. In the microgrid, the PV unit in microgrid usually operates in the maximum power point tracking (MPPT) state [4]. And BES is connected to the DC bus through its interface DC/DC converter, which can smooth out the fluctuations generated by the PV unit and the load, thereby maintaining the power balance in the DC microgrid and the stability of the DC bus voltage. The control strategies of the DC/DC converter of the energy storage interface usually use constant voltage control or droop control. Both proportional-integral (PI)-based control strategies have a positive effect on maintaining the stability of the DC bus voltage. However, due to the lack of inertia and damping of the converter, the voltage stabilization effect of BES is limited and the DC microgrid is still a low-inertia network. Intermittent fluctuations from the PV unit and load switching can result in sudden changes in the DC bus voltage, which significantly impact the stability of the DC microgrid system and the voltage quality [5].

To address the aforementioned issues, experts both domestically and internationally have proposed various types of inertia control strategies, mainly including virtual element control [6–9], virtual DC generator (VDG) control [10–17], and analogous virtual generator (AVSG) control [18–22]. Virtual element control is often used in the form of electronic components for inertial enhancement. Adib et al. proposed an adaptive virtual impedance control strategy to improve system inertia by adjusting the load input impedance [6]. Li et al. [7] used virtual capacitance control to improve the performance of the system transient response, but this control still produced a certain degree of voltage fluctuation during the initial stages of disturbance. Similarly, the research of Ahmed et al. [8,9] also

showed that the virtual element inertial control can improve system stability. As a single variable control strategy, virtual element control has a simple structure, but it has relatively poor robustness to system parameter changes or external interference. Therefore, with the evolution of inertia control strategies, multi-variable and higher-performing virtual motor control technologies, including the VDG and the AVSG, have been proposed.

The VDG control simulating the characteristics of the DC generator is used in the interface converter of the DC microgrid side to provide inertia and damping. The VDG control can be applied to the converter of the load side to reduce DC bus voltage fluctuation caused by disturbance of the load [10,11]. He et al. [12] proposed a control strategy applying the VDG control to the source-side converter of the DC microgrid to effectively reduce the influence caused by power fluctuation. Furthermore, as an inertia control strategy, the VDG control is commonly used in the energy storage side of the DC microgrid system. The VDG control not only adjusts the power support function of energy storage devices to fully utilize their performance but also stabilizes the DC bus voltage. Tan et al. [13,14] applied the VDG control to the energy storage interface converter to enhance the inertial support capability and power calming effect of the energy storage unit. However, as a multi-variable control strategy introducing inertia and damping, the VDG control lacks inherent droop characteristics [15–17]. The direct utilization of the VDG control only meets the requirements for maintaining constant voltage control of the energy storage interface converter, while it fails to address the demands of droop control. To impart droop characteristics to the DC bus voltage, which is better suited for accommodating multiple energy storage units in the DC microgrid in the future, the AVSG control strategy is introduced.

By drawing inspiration from the VSG control concept in the AC microgrid, the AVSG control incorporates inertia, damping, and droop characteristics, and has a simple structure. It is well-suited for DC microgrids and demonstrates significant effectiveness in stabilizing DC bus voltage. Cao et al. [18] proposed a variable-structure AVSG control strategy for DC microgrid multi-port converters. Zhu et al. [19,20] designed two AVSG control strategies for the power electronic converters and both control strategies have shown excellent voltage regulation performance. The converter controlled by the AVSG can smooth the voltage fluctuation in the DC microgrid to a certain extent. However, during instances of large external power disturbances, especially when random fluctuations arise within the microgrid, the fixed inertia and damping parameters limit the flexibility of the DC microgrid's inertia. As a result, there may still be a large fluctuation of the DC bus voltage in the transient process, affecting the stability of the system. To tackle this issue, the parameter adaptive control method is introduced and has been proven effective in improving the flexibility of the DC microgrid's inertia. At present, there have been some research results on the AVSG adaptive control. Cao et al. [21,22] employed two adaptive control approaches for inertia and damping based on distinct AVSG control structures, and both adaptive controls exhibited certain improvements in comparison to the original control. However, Cao et al. [21] solely focused on the impact of load fluctuation, and the effectiveness of the adaptive control is unsatisfactory. Zeng et al. [22] considered the impacts of the photovoltaic power and load power under the step conditions, but the designed adaptive control lacks universality and presents complexity. In reality, scenarios involving random power fluctuations more closely resemble the actual operating conditions of the DC microgrid. Examples include short-term random shifts in solar irradiance and frequent load switching, both of which require consideration.

Therefore, according to the above analysis, the study conducted encompasses the following:

(1) Through theoretical analysis and equation derivation, the AVSG control is introduced into the DC/DC converter of the BES interface in the DC microgrid.

(2) By analyzing the inertia effects of the AVSG control parameters that meet system stability, a universally applicable and simple adaptive parameter control method is designed.

(3) In the scenarios involving both step power fluctuation and random power fluctuation of the PV and load, the correctness and effectiveness of the AVSG adaptive control strategy are proved. Furthermore, the role of the voltage rate of change tracking coefficient in AVSG adaptive control is discussed.

2 Structure of DC Microgrid with PV and BES

The DC microgrid in this study comprises the photovoltaic (PV) unit, the battery energy storage (BES) unit, the load unit, and the corresponding interface converters, as illustrated in Fig. 1. The PV unit operates in the MPPT mode to output the photovoltaic power. The load units are connected to the DC bus and output the load power.

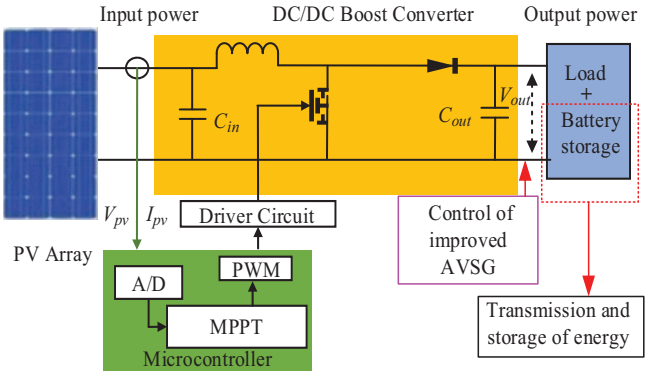

Figure 1: The overall framework of DC microgrid

When the step or random fluctuations occur in the photovoltaic output power and the load output power within the microgrid, the BES can stabilize the certain system power and stabilize the DC bus voltage through the energy storage interface DC/DC converter. However, the introduction of the BES does not fundamentally address the issue of low system inertia in the DC microgrid. Therefore, this paper adopts the AVSG control to tackle the problem of insufficient system inertia. Besides, introducing an adaptive and enhanced control strategy for the AVSG control aims to provide flexible and improved inertial support, enhancing the stability and robustness of the DC bus voltage in response to the power changes within the DC microgrid.

3 Adaptive Control Strategy for DC Microgrid Based on AVSG

3.1 AVSG Control Principle

In the AC microgrid, the VSG control is usually applied to the DC/AC converter to improve the inertia. The active power-frequency $P-\omega$ link of the control structure simulates the inertia, damping, and primary frequency modulation characteristics of the synchronous generator, and the original VSG equation is shown in Eq. (1).

$$\begin{cases} P_{\text{set}} - P_{\text{e}} - P_{\text{D}} = J\omega\dfrac{\text{d}\omega}{\text{d}t} \approx J\omega_{\text{N}}\dfrac{\text{d}\omega}{\text{d}t} \\ P_{\text{D}} = D_{\text{p}}\left(\omega - \omega_{N}\right) \end{cases} \tag{1}$$

where J and D_p are the moments of inertia and damping coefficient, respectively, P_{set} is the $P-\omega$ droop control output power, P_e is the output electromagnetic power, P_D is the damping power, ω is the angular frequency, and ω_N is the rated value of ω. Based on the control structure of Eq. (1), ω_N is introduced into the inertia link, the $P-\omega$ droop frequency modulation link, and the damping link. ω_c acts as the feedback signal of the frequency modulation link, and the new VSG control equation is shown in Eq. (2).

$$J\omega\frac{\mathrm{d}(\omega-\omega_N)}{\mathrm{d}t}=k(\omega_N-\omega_c)+P_N-P_e-D_p(\omega-\omega_N) \tag{2}$$

where P_N is the rated power of $P-\omega$ droop control, k is the droop coefficient, and ω_c is the angular frequency of the DC bus. According to Eq. (2), when the grid frequency changes suddenly, k is used for the primary frequency modulation, D_p is used to suppress the frequency oscillation, and J can make the converter control the active power output under the adjustment of VSG, thereby achieving the effect of suppressing frequency changes. The energy W_r stored in J is shown in Eq. (3).

$$W_r=\frac{1}{2}J\omega^2 \tag{3}$$

Drawing inspiration from the concept of the VSG in the AC microgrid, the AVSG control is implemented in the DC microgrid. Analogous to the $P-\omega$ droop control in the AC microgrid, the droop control that utilizes current to suppress the voltage fluctuation is implemented in the DC microgrid. Analogous to Eq. (3), in the energy storage interface DC/DC converter, the energy can be stored by paralleling the virtual capacitance C_v, acting as the moment of inertia J in the AC microgrid. The energy W_c stored in C_v is shown in Eq. (4).

$$W_c=\frac{1}{2}C_v u_{dc}^2 \tag{4}$$

where u_{dc} is the DC bus voltage, which is also the output voltage of the DC/DC converter in this paper. The remaining variables associated with the DC/DC converter follow a similar pattern.

The main variable in the AC microgrid is frequency, while in the DC microgrid, the DC bus voltage is the sole indicator to measure the power balance and the stability of the system. Inertia and damping represent the ability to suppress the sudden changes and oscillations in the DC bus voltage. The DC/DC converter lacking inertia features on the DC side is too sensitive to the response of the DC bus voltage, which can cause voltage sudden changes or system instability when responding to external power fluctuations. The introduction of a virtual capacitance with voltage-stabilizing properties slows down voltage changes by utilizing the stored energy. By analogy with the relationship between frequency and power in Eq. (2), the energy stored in J is substituted with the energy stored in C_v, while factoring in the damping effect for voltage oscillation suppression, the control equation for virtual capacitance current is shown in Eq. (5).

$$\Delta i=C_v\frac{\mathrm{d}u_{dc}^*}{\mathrm{d}t}=i_{set}-i_{dc}-i_d \tag{5}$$

where u_{dc}^* is the output voltage of the AVSG, and Δi, i_{set}, i_{dc} and i_d are virtual capacitance current, the droop control input current, the DC bus current, and damping current, respectively.

Based on the above analysis, the analogous relationships exist between the DC/AC converter with the VSG in the AC microgrid and the DC/DC converter with the AVSG in the DC microgrid. The corresponding analog parameters of the AC microgrid and the DC microgrid are illustrated in Table 1.

Table 1: Analogy between the AC microgrid and the DC microgrid

Analogous items	The AC microgrid with the VSG	The DC microgrid with the AVSG
Droop equation	$\omega - P_e$	$u_{dc} - i_0$
Objective of control	ω	u_{dc}
Output of control	P_e	i_0
Inertia of system	J	C_v
Energy relationship	$0.5J\omega^2$	$0.5C_v{u_{dc}}^2$

According to the correspondence between the variables between the DC microgrid and the AC microgrid in Table 1, and the analogy of Eqs. (2) and (5), and make adjustments to some variables, the AVSG control equation is shown in Eq. (6).

$$k_{droop}\left(u_N - u_{dc}\right) - i_{dc} - D_p\left(u_{dc}^* - u_{dc}\right) = C_v\frac{\mathrm{d}\left(u_{dc}^* - u_N\right)}{\mathrm{d}t} \tag{6}$$

where k_{droop} is droop coefficient of the AVSG control; u_N is the rated voltage of the AVSG.

Fig. 2 shows the control block diagram of the energy storage system with the AVSG, which is composed of the BESS (Battery Energy Storage System), the current tracking module, and the AVSG control module. The output voltage u_{dc}^* of the AVSG control module is used as a reference value for the voltage outer loop. In order to eliminate voltage steady-state errors, the outer loop uses the voltage PI controller to make the converter DC side voltage u_{dc} track the reference value u_{dc}^* all the time. The output current i_{dc}^* outputs the signals to the switch tubes S_1 and S_2 of the DC/DC converter through the current tracking module to achieve the control purpose.

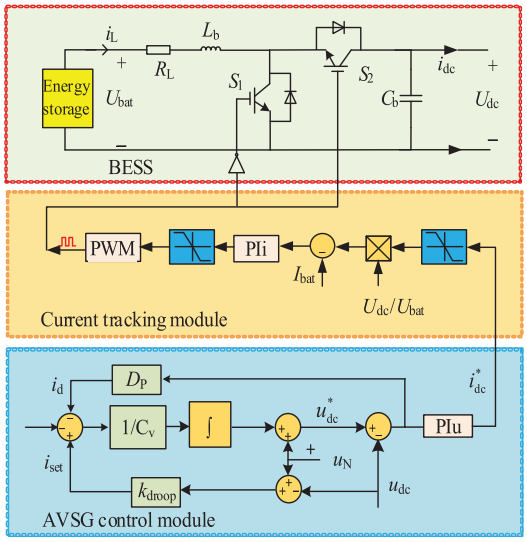

Figure 2: Control block diagram of energy storage system with AVSG

3.2 AVSG Equivalent Model

As shown in Fig. 3, the AVSG equivalent model is established on the basis of the droop control equivalent model, and the equivalent components of the AVSG control are introduced. The impedance R_d represents the droop coefficient, the inductance L_{PI} represents the voltage PI controller, C_v is the virtual capacitance, and $-D_p u_L$ is the controllable current source. Compared with the droop control, the AVSG control introduces inertia and damping to the system, thereby improving the voltage quality of the microgrid.

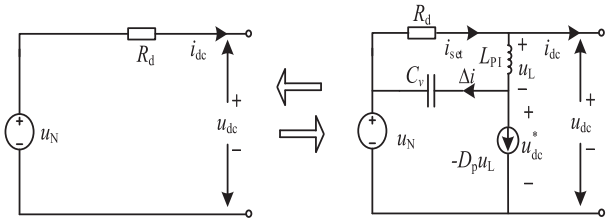

Figure 3: AVSG equivalent model

3.3 AVSG Small Signal Modeling and Inertial Trend Analysis

In order to analyze the specific control effect of the energy storage interface DC/DC converter after the introduction of the AVSG control, suppose the duty cycle of the DC/DC converter is d, and the state space equation is shown in Eq. (7).

$$\begin{cases} \dot{x} = C_1 x + C_2 u \\ x = [i_L u_{dc}]^T \\ u = [u_{bat} i_{dc}]^T \end{cases} \tag{7}$$

where x and u are state variables, u_{bat} and i_L are respectively the input voltage and input current of the energy storage interface DC/DC converter, and u_{dc} and i_{dc} are respectively the output voltage and output current of the energy storage interface DC/DC converter. The matrices $C_1$and C_2 are respectively are shown in Eq. (8).

$$C_1 = \begin{bmatrix} \dfrac{R_L}{L_b} & \dfrac{1-d}{C_b} \\ \dfrac{1-d_b}{C_b} & 0 \end{bmatrix} C_2 = \begin{bmatrix} \dfrac{1}{L_b} & 0 \\ 0 & -\dfrac{1}{C_b} \end{bmatrix} \tag{8}$$

The small-signal linearization of the state average equation is carried out, and the disturbance is introduced near the steady-state operating point, and the instantaneous values of the corresponding DC/DC converter variables are shown in Eq. (9).

$$\begin{cases} i_L = I_L + \Delta i_L \\ u_{dc} = U_{dc} + \Delta u_{dc} \\ u_{bat} = U_{bat} + \Delta u_{bat} \\ d = D + \Delta d \\ i_{dc} = I_{dc} + \Delta i_{dc} \end{cases} \tag{9}$$

where Δi_L, Δu_{dc}, Δu_{bat}, Δd and Δi_{bat} represent the corresponding small signal disturbance, and I_L, U_{dc}, U_{bat}, D and I_{dc} represent the steady-state values of the corresponding variables. The small signal equation after neglecting the quadratic disturbance is shown in Eq. (10).

$$\begin{cases} sC\Delta u_{dc} = (1-D)\,\Delta i_L - I_L\Delta d - \Delta i_{dc} \\ sC\Delta i_L = \Delta u_{bat} - R_L\Delta i_L - (1-D)\,\Delta u_{dc} + U_{dc}\Delta d \end{cases} \tag{10}$$

By sorting out the small signal equation of Eq. (10), the relevant transformation can be deduced. The main transfer function of the DC/DC converter is shown in Eq. (11).

$$\begin{cases} G_{ii}(s) = \dfrac{\Delta i_L(s)}{\Delta i_{dc}(s)} = \dfrac{1-D}{C_b L_b s^2 + C_b R_L s + (1-D)^2} \\ G_{id}(s) = \dfrac{\Delta i_L(s)}{\Delta d(s)} = -\dfrac{CU_{dc}s + (1-D)\,I_L}{C_b L_b s^2 + C_b R_L s + (1-D)^2} \\ G_{ud}(s) = \dfrac{\Delta u_{dc}(s)}{\Delta d(s)} = \dfrac{-L_b i_{Lb} s - R_L i_L + (1-D)\,U_{dc}}{C_b L_b s^2 + C_b R_L s + (1-D)^2} \\ G_{iu}(s) = \dfrac{\Delta i_{dc}(s)}{\Delta u_{dc}(s)} = -\dfrac{-L_b s - R_L}{C_b L_b s^2 + C_b R_L s + (1-D)^2} \end{cases} \tag{11}$$

where $G_{ii}(s)$ is the transfer function from the output current to the input current, $G_{id}(s)$ is the transferfunction from the duty cycle to the input current, $G_{ud}(s)$ is the transfer function from the duty cycle to the output voltage and $G_{iu}(s)$ is the the output voltage to the input current.

Neglecting energy losses, the power balance on both sides of the energy storage interface DC-DC converter is depicted in Eq. (12).

$$u_{bat} i_L = u_{dc} i_{dc} \tag{12}$$

Linearize the small-signal equation of Eq. (12) and neglect the quadratic disturbance, as shown in Eq. (13).

$$I_L\Delta u_{bat} + U_{bat}\Delta I_L = u_{dc} = I_{dc}\Delta u_{dc} + U_{dc}\Delta i_{dc} \tag{13}$$

According to the superposition theorem, the small signal disturbance Δu_{bat} and Δu_{dc} in Eq. (13) can be neglected. The resulting simplified transfer function between Δi_{dc} and Δi_L is presented in Eq. (14).

$$G_{iiL} = \frac{\Delta i_L(s)}{\Delta i_{dc}(s)} = \frac{U_{dc}}{U_{bat}} \tag{14}$$

Laplace transform and small-signal linearization are applied to Eq. (6), yielding the small-signal model controlled by the AVSG as shown in Eq. (15).

$$-k_{droop}\Delta u_{dc}(s) - \Delta i_{dc}(s) - D_p\left[\Delta u^*_{dc}(s) - \Delta u_{dc}(s)\right] = C_v s\Delta u^*_{dc}(s) \tag{15}$$

The AVSG small-signal model of the established energy storage DC/DC converter is shown in Fig. 4. The voltage outer loop and current inner loop adopt the PI control, as shown in Eq. (16).

$$\begin{cases} G_u = k_{pv} + k_{iv}/s \\ G_i = k_{pi} + k_{ii}/s \end{cases} \tag{16}$$

where k_{pu} and k_{iu} are the PI parameters of the converter voltage outer loop, and k_{pi} and k_{ii} are the PI parameters of the converter current inner loop.

The AVSG small signal model of the energy storage DC/DC converter is shown in Fig. 4, and the AVSG output current disturbance is shown in Eq. (17).

$$\Delta i_{dc}^{*}(s)=\left(k_{pv}+k_{iv}/s\right)\left[\Delta u_{dc}^{*}(s)-\Delta u_{dc}(s)\right] \tag{17}$$

Combined with the operating characteristics of the PI controller, $\Delta i_{dc}(s)$ is approximate to $\Delta i_{dc}^{*}(s)$, and Eq. (17) is substituted into Eq. (15). And the equivalent droop coefficient of AVSG control is shown in Eq. (18).

$$m=\lim_{s\to 0}\left(\frac{\Delta u_{dc}(s)}{\Delta i_{dc}(s)}\right)=-\frac{1}{k_{droop}} \tag{18}$$

According to Eq. (18), the droop coefficient k_{droop} determines its equivalent droop coefficient m. Since droop control involves differentiating the voltage, k_{droop} will impact the bus voltage offset when the power of the microgrid changes. Based on Eqs. (15) and (18), and taking into account the composition of the AVSG control structure along with the derivation of its small signal model, the approximate relationship between the ratio of $\Delta u_{dc}(s)$ and $\Delta i_{dc}(s)$ is depicted in Eq. (19).

$$\frac{\Delta u_{dc}(s)}{\Delta i_{dc}(s)}\approx\frac{m}{\left(C_v/D_p\right)s+1} \tag{19}$$

This article only requires a brief analysis of the relationship between the inertial parameters of the AVSG and the inertia of the DC microgrid, along with the design of the parameter adaptive equation. Fig. 4 reveals that, beyond the main pathway, the AVSG closed-loop system is also influenced by two additional secondary paths L_1 and L_2, leading to a relatively intricate analysis. Moreover, the dynamic behavior of the higher-order AVSG system can be directly inferred from the dynamic performance index of the first-order inertial system [20]. As a result, the equivalent first-order transfer function $TF(s)$ of the AVSG closed-loop system is represented in Eq. (20).

$$TF(s)=\frac{\Delta u_{dc}(s)}{-\Delta i_{dc}(s)}\approx\frac{1/k_{droop}}{\left(C_v/D_p\right)s+1},\tau=C_v/D_p,|m|=1/k_{droop} \tag{20}$$

where τ is the inertial time constant. According to Eq. (20), the unit step response curve of the AVSG control parameter variations can be plotted. It can be seen from Fig. 5a that the larger the C_v, the smaller the change of the DC bus voltage perunit time, the longer the time for the DC bus voltage to stabilize, the stronger the inertia of the DC microgrid system. The smaller the C_v, the shorter the time for the DC bus voltage to stabilize, the smaller the inertia of the DC microgrid. In addition, in the equation, $\tau=C_v/D_p$, which reflects the size of the inertia of the system, and C_v is proportional to the inertial time constant τ.

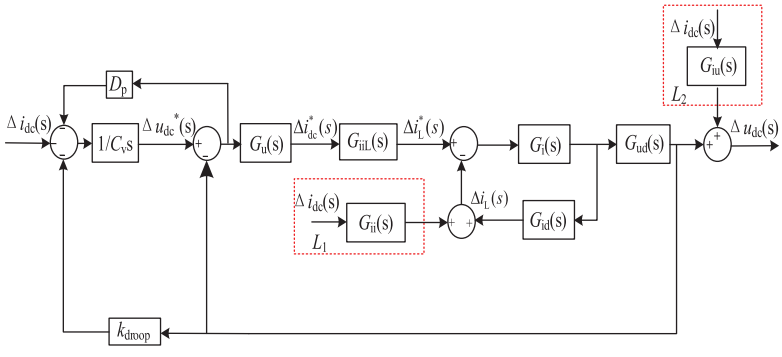

Figure 4: AVSG small signal modeling of energy storage DC/DC converter

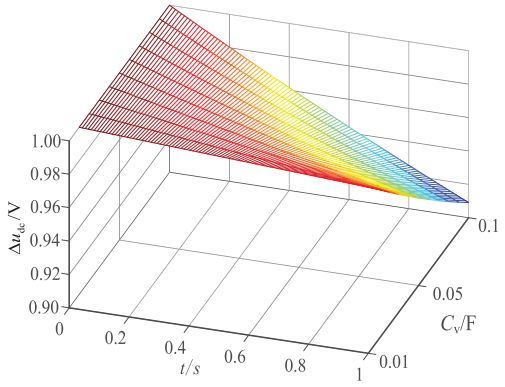

(a) Unit step response of $TF(s)$ when C_v changes

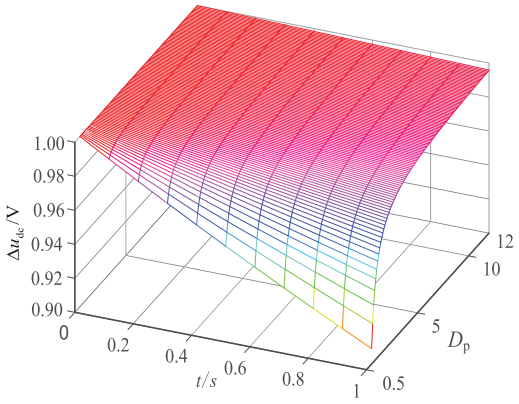

(b) Unit step response of $TF(s)$ when D_p changes

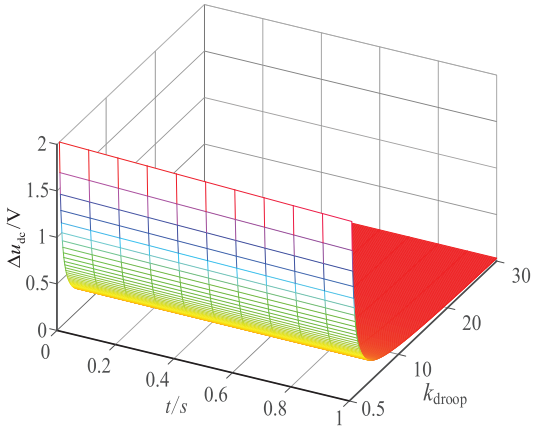

(c) Unit step response of $TF(s)$ when k_{droop} changes

Figure 5: Unit step response curve of AVSG control parameter changes

It can be seen from Fig. 5b that a suitable decrease in D_p can extend the time required for voltage stabilization, thereby enhancing the inertia of the DC microgrid system. Conversely, an increase in D_p weakens the inertia. Both Figs. 5a and 5b illustrate that C_v and D_p can impact the inertia, being components of the τ function. Eq. (20) indicates that k_{droop} is not governed by the τ function and is not correlated with the inertia trend. Nonetheless, as shown in Fig. 5c, it is evident that k_{droop} influences the voltage offset, showcasing a gradual decrease. Hence, an adaptive adjustments in C_v and D_p values can modify the inertia of the microgrid system.

3.4 AVSG Adaptive Control and System Stability Analysis

To enable the AVSG control to dynamically adjust C_v and D_p in response to changes in the DC bus voltage, C_v and D_p should be formulated as functions of the rate of voltage change. Therefore, the voltage change rate tracking coefficients A and B are introduced, and $|du_{dc}/dt| > k_v$ is used as a limiting condition to determine whether the DC bus voltage fluctuates. The flexible adjustment of C_v and D_p can improve the inertia of the DC microgrid system and effectively address the voltage fluctuations

generated by the distributed power sources and load power changes. Based on the aforementioned impact of C_v and D_p trends on the inertia of the DC microgrid, the adaptive parameter conditions are designed, as depicted in Eqs. (21) and (22).

$$\begin{cases} C_v = C_{v0} & (|u_{dc} - u_N| \le k_u) \cap (|du_{dc}/dt| \le k_v) \\ C_v = C_{v0} + A\,|du_{dc}/dt| & |du_{dc}/dt| > k_v \end{cases} \tag{21}$$

$$\begin{cases} D_p = D_{p0} & (|u_{dc} - u_N| \le k_u) \cap (|du_{dc}/dt| \le k_v) \\ D_p = D_{p0} - B\,|du_{dc}/dt| & |du_{dc}/dt| > k_v \end{cases} \tag{22}$$

where C_{v0} and D_{p0} are the initial virtual capacitance and damping coefficient, respectively, and A and B are the voltage conversion rate tracking coefficients, which can be selected according to the actual situation, and k_u and k_v are the minimum voltage change and voltage change rate that are allowed to fluctuate. This article sets the value of k_u and k_v to 0 for simplifying.

When performing parameter adaptive optimization, a high-pass filter (HPF) is used to mitigate the disturbance caused by introducing the differential link to obtain the voltage change rate within the system. This approach facilitates the acquisition of the voltage change rate. Simultaneously, to prevent output voltage oscillations resulting from sudden changes in C_v and D_p, a low-pass filter (LPF) has been added to the output terminals of C_v and D_p, respectively. The block diagram illustrating the adaptive control of the AVSG is shown in Fig. 6.

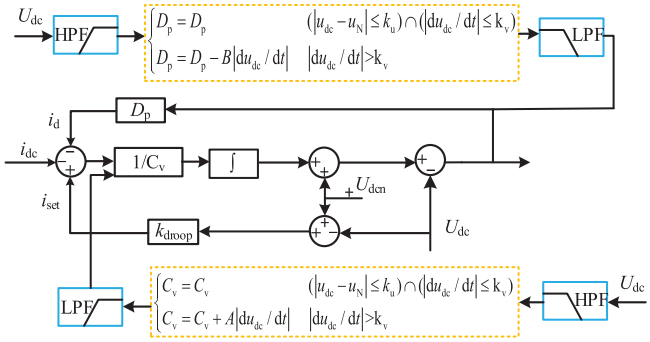

Figure 6: The block diagram of AVSG adaptive control

To simplify the analysis, ignoring the influence caused by two secondary paths L_1 and L_2 in Fig. 4, the closed-loop transfer function $TF_{ff}(s)$ between $\Delta u_{dc}(s)$ and $-\Delta i_{dc}(s)$ is shown in Eq. (23).

$$TF_{ff} = \Delta u_{dc}(s)/(-\Delta i_{dc}(s)) = (G_{ud}G_iG_uG_{ii})/\left[\left(C_v s + D_p\right)(1 + G_{id}G_i) + \left(k_{droop} + C_v s\right)G_{ud}G_iG_uG_{ii}\right] \tag{23}$$

By analyzing the closed loop pole distribution trends of C_v, D_p and k_{droop} changes, a rough range of the AVSG control parameters that ensure system stability can be determined.

As shown in Fig. 7a, in addition to the fixed poles that have satisfied stability, it is also necessary to analyze the influence of changing poles on the system stability. With the increase of C_v, the poles labeled as P_{11}, P_{12} and P_{13} are from left to right. P_{11} gradually moves toward the imaginary axis, weakening the system stability. P_{12} gradually moves away from the imaginary axis, enhancing the system stability. As the dominant pole closest to the imaginary axis, P_{13} moves toward the imaginary axis, and the system stability tends to weaken, but it does not enter the right half-plane, and the entire system remains stable. Similarly, in Figs. 7b and 7c, the dominant poles P_{23}, P_{32}, and P_{33} closest to the imaginary axis determine the trend of system stability. The larger the values of D_p and k_{droop}, the

closer their poles are to the intersection of the left half-plane and the right half-plane, and the worse the overall system stability will be.

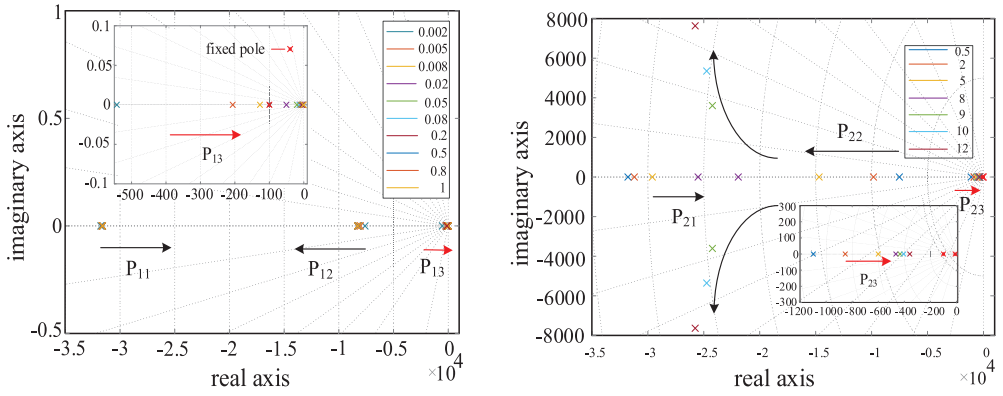

(a) Pole Distribution of $TF_{ff}(s)$ When C_v Changes (b) Pole Distribution of $TF_{ff}(s)$ When D_p Changes

(c) The pole Distribution of $TF_{ff}(s)$ When k_{droop} Changes

Figure 7: Closed loop pole distribution diagram of AVSG parameters

4 Simulation Analysis

4.1 Simulation Model Construction

To validate the efficacy of the proposed control strategy, a simulation platform is constructed using MATLAB/Simulink, as depicted in Fig. 1. The PV unit operates at a rated temperature of 25°C, with an initial solar irradiance of 600 W/m^2. The parameters of the DC microgrid system are provided in Table 2.

Table 2: The parameters of the DC microgrid system

Paramater	Value	Unit
Energy storage converter input voltage (U_{in})	244.15	/V
Energy storage converter output voltage (U_{dc})	399.75	/V

(Continued)

Table 2 (continued)

Paramater	Value	Unit
Battery capacity (*SOC*)	80.15	%
DC bus rated volatge (U_N)	400	/V
Equivalent inductance of energy storage side (L_b)	0.0013	/H
Energy storage side equivalent resistance (R_L)	0.15	/Ω
Energy storage side equivalent capacitance (C_b)	0.005	/F
Load switching initial resistance (R)	45	/Ω
Switching frequency (f_s)	50	/HZ
Coefficient of current-loop of energystorage converter (k_{pi}/k_{ii})	0.1/10	
Coefficient of voltage-loop of energystorage converter (k_{pv}/k_{iv})	20/200	

4.2 Simulation Waveform under AVSG Control Strategy

4.2.1 The Effect of AVSG Control Parameters on DC Bus Voltage

Scenario 1: in this scenario, the solar irradiance is changed, transitioning from the initial value of 600 to 1000 W/m² at 1.5 s. Fig. 8 illustrates the simulated waveforms of the DC bus voltage under varying conditions of C_v, D_p and k_{droop}.

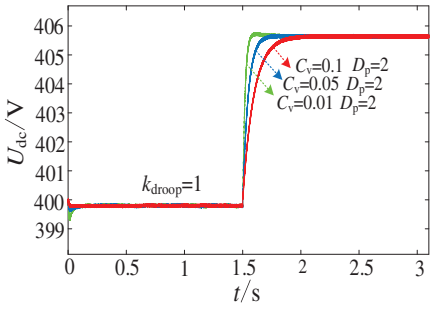

(a) DC bus voltage when C_v changes

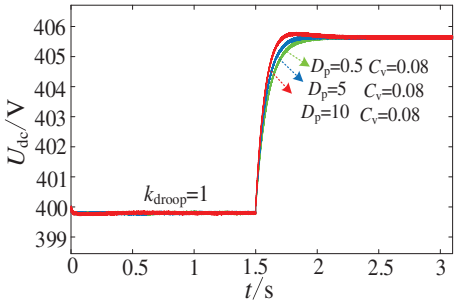

(b) DC bus voltage when D_p changes

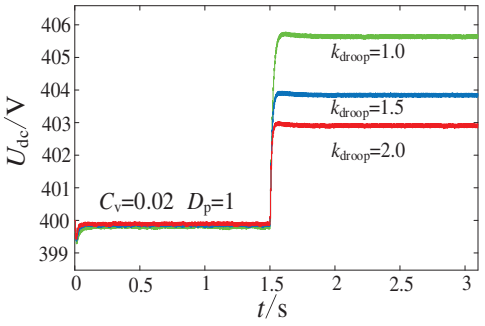

(c) DC bus voltage when k_{droop} changes

Figure 8: Effect of AVSG control parameters on DC bus voltage

In this study, the degree of the fluctuation and dynamic change in the DC bus voltage are used as indicators to reflect the inertia strength of the DC microgrid, as demonstrated in Fig. 9c. When power step disturbances manifest within the microgrid, the inertia of the microgrid is predominantly revealed through the dynamic changes of the DC bus voltage. Moreover, the inertia can also be indirectly reflected by the dynamic response time of the DC bus voltage. The slower the dynamic change of the DC bus voltage, the longer the dynamic response time, and the stronger the inertia of the microgrid. As depicted in Fig. 8a, the dynamic change of the DC bus voltage differs based on different values of C_v. A larger value of C_v improves the dynamic change of the voltage and extends dynamic response time, leading to increased stability of the DC bus voltage and the inertia of the system. In Fig. 8b, the impact of D_p on inertia is contrary to that of C_v and decreasing D_p enhances the inertia. In Fig. 8c, k_{droop} does not affect the system inertia, but an increase in k_{droop} leads to a reduction in the offset of the DC bus voltage. The value of k_{droop} is not the focus of this paper. In the control of the energy storage equipment, k_{droop} is typically set as a constant value.

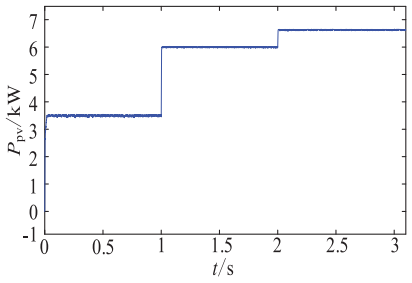

(a) Output Power of Photovoltaic Unit

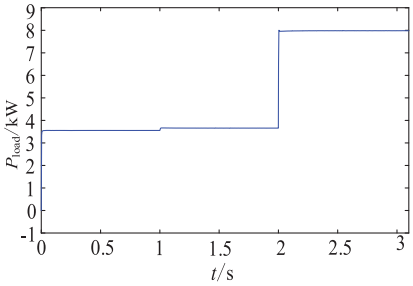

(b) Output Power of Load

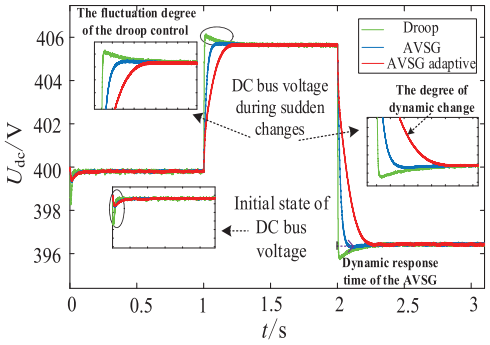

(c) DC Bus Voltage When Output Power Changes

Figure 9: Effect of different control strategies on DC bus voltage

4.2.2 The Effects of Different Control Strategies on DC Bus Voltage

Scenario 2: The initial solar irradiance is 600 W/m^2, which increases to 1000 W/m^2 at 1 s and further rises to 1100 W/m^2 at 2 s. The corresponding changes in photovoltaic output power are depicted in Fig. 9a. In Fig. 9b, the initial load power consumption is 3.5 kW. At 1 s, the load power consumption slightly increases to 3.6 kW. At 2 s, a 35 Ω load is introduced, causing the power to rise to 8 kW. To facilitate clear observation of the control effects, the following initial parameters are chosen for the AVSG: $C_v = 0.02$ F, $D_p = 1$, and $k_{droop} = 1$. It is important to note that the values of the voltage tracking coefficients A and B should be selected to keep C_v and D_p within a parameter range that maintains

system stability. For this purpose, the voltage change rate tracking coefficients are set as $A = 0.1$ and $B = 4$. The impact of the different control strategies on the DC bus voltage is demonstrated in Fig. 9c.

As depicted in Fig. 9c, it is clear that the AVSG control can effectively mitigate the initial voltage fluctuations of the DC bus under droop control. When photovoltaic and load power shift at 1 and 2 s, the AVSG control augments droop control with fixed C_v and D_p. This improvement strengthens the resistance of the DC bus to sudden voltage changes, prolongs dynamic response time, and enhances the system inertia. In comparison to the AVSG control, the AVSG adaptive control readjusts the values of C_v and D_p, enabling C_v and D_p to adapt to changes in the DC bus voltage. Therefore, the dynamic change degree of the DC bus voltage has been significantly improved, which shows the inertial capability of the system has been further improved.

Fig. 10 illustrates that when the rapid changes manifest in the photovoltaic power and load power, corresponding fluctuations arise in the DC bus voltage and its rate of change, and the parameter adjustments of C_v and D_p in the AVSG adaptive control.

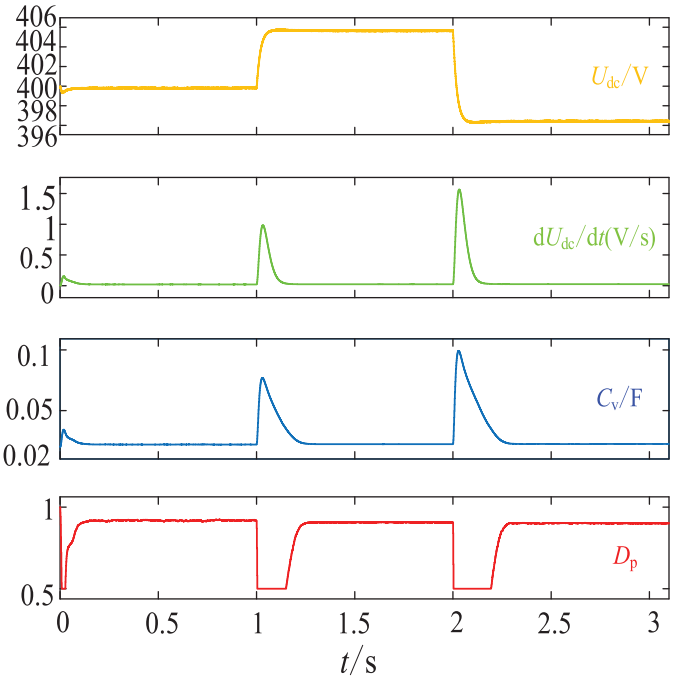

Figure 10: Parameter changes of AVSG adaptive control

4.2.3 The Effects of Different Control Strategies on the Main Variables of Battery

Analyzing the effects of different control strategies on the key parameters of the battery in Scenario 2.

Observing Figs. 11a and 11b, it becomes evident that changes in microgrid power demand lead to battery overshooting under traditional droop control, which is harmful to the battery's lifespan. In contrast, both the AVSG control and the AVSG adaptive control eliminate this overshoot phenomenon. The AVSG adaptive control makes the transient change of battery power more apparent, and the battery power responds faster, thereby enhancing the battery's power support capability. Fig. 11c shows the battery *SOC* difference, which is defined as the gap between the changing value

and the initial value. Taking t = 2 s as an example, the rate change of *SOC* difference under the AVSG adaptive control is the fastest, indicating that the AVSG adaptive control maximizes the utilization of battery performance.

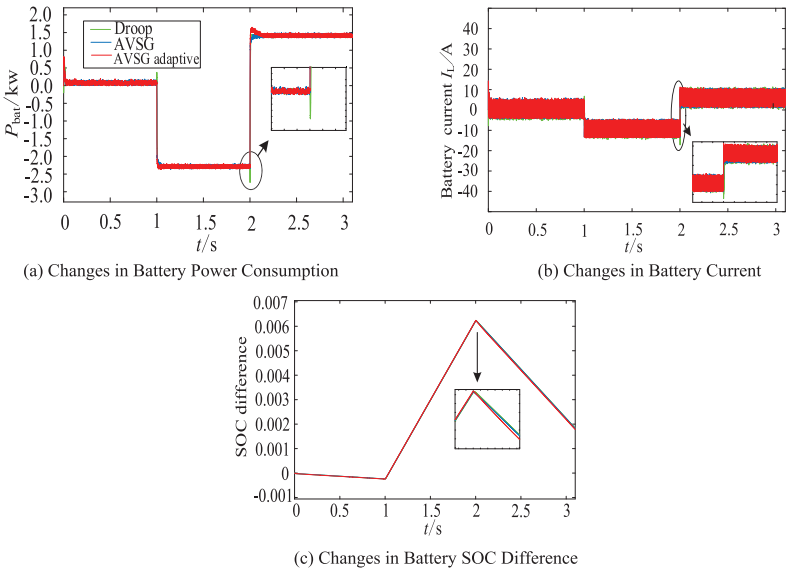

(a) Changes in Battery Power Consumption

(b) Changes in Battery Current

(c) Changes in Battery SOC Difference

Figure 11: Changes in key battery parameters under different control strategies

4.2.4 Simulation Waveforms of Different Control Strategies in a Simulated Natural Environment

Scenario 3: Simulating the fluctuation of short-term solar irradiance under natural conditions, with the ambient temperature held at 25°C, the values associated with the AVSG control parameters remain consistent with those in Scenario 2, and the effect of different control strategies on the DC bus voltage is depicted in Fig. 12a.

The random load fluctuations exhibit a similar behavior to the photovoltaic fluctuations, so this scenario will not be elaborated upon. In the case of power random fluctuations in the DC microgrid, besides using the dynamic variation of the DC bus voltage as an indicator, the inertia strength of the DC microgrid can be more clearly reflected through the degree of fluctuation in the DC bus voltage. Therefore, the fluctuation of the DC bus voltage is considered the primary indicator. The smaller the voltage fluctuation, the stronger the anti-interference ability of the bus voltage, the larger the inertia of the DC microgrid, the more stable the system. Fig. 12b reveals distinctions in the DC bus voltage waveform under the three control strategies. The degree of fluctuation is attenuated to some extent through the application of the AVSG control. However, there is still room for improvement in the fluctuation suppression effect of the AVSG control on the DC bus voltage. By applying the adaptive control to C_v and D_p, it is possible to more flexibly reduce the fluctuation of the DC bus voltage, thereby achieving an even better and flexible system inertia.

In Fig. 13, the significant parameter changes in the AVSG adaptive control occur during periods of random short-term solar irradiance fluctuations, with the voltage change rate tracking coefficients A and B playing a crucial role in the adaptive control of C_v and D_p.

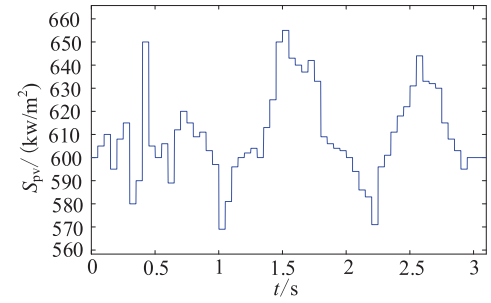

(a) Random Fluctuation Process of Solar Irradiance

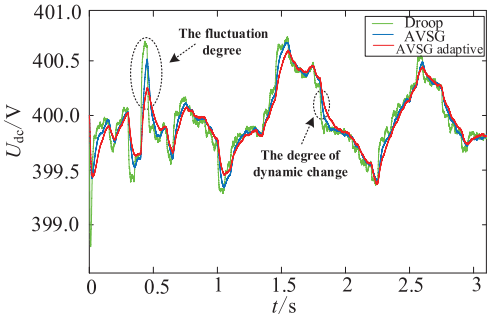

(b) The Effect of Different Control Strategies on DC Bus Voltage

Figure 12: Simulation waveforms in a simulated natural environment

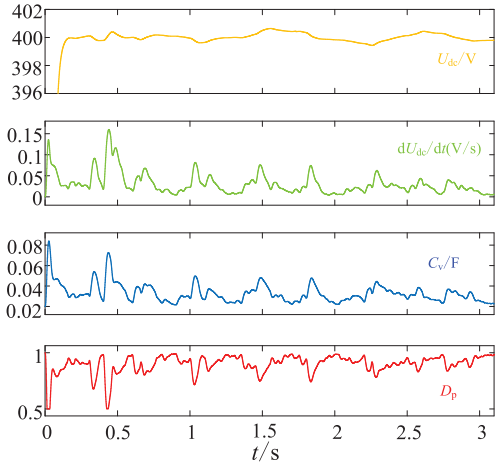

Figure 13: Parameter changes of AVSG adaptive control

4.3 The Effects of the Values of A and B on the AVSG

The effects of the voltage change rate tracking coefficients A and B on the AVSG are still examined in Scenario 2. The roles of A and B in Scenario 3 are similar to those in Scenario 2, eliminating the need for further explanation. Whenever there is a change in the power of the DC microgrid, the AVSG adaptive control can recalibrate the values of C_v and D_p by adjusting A and B. As illustrated in Figs. 14a and 14b, the waveform variations of C_v and D_p can be observed with different values of A and B.

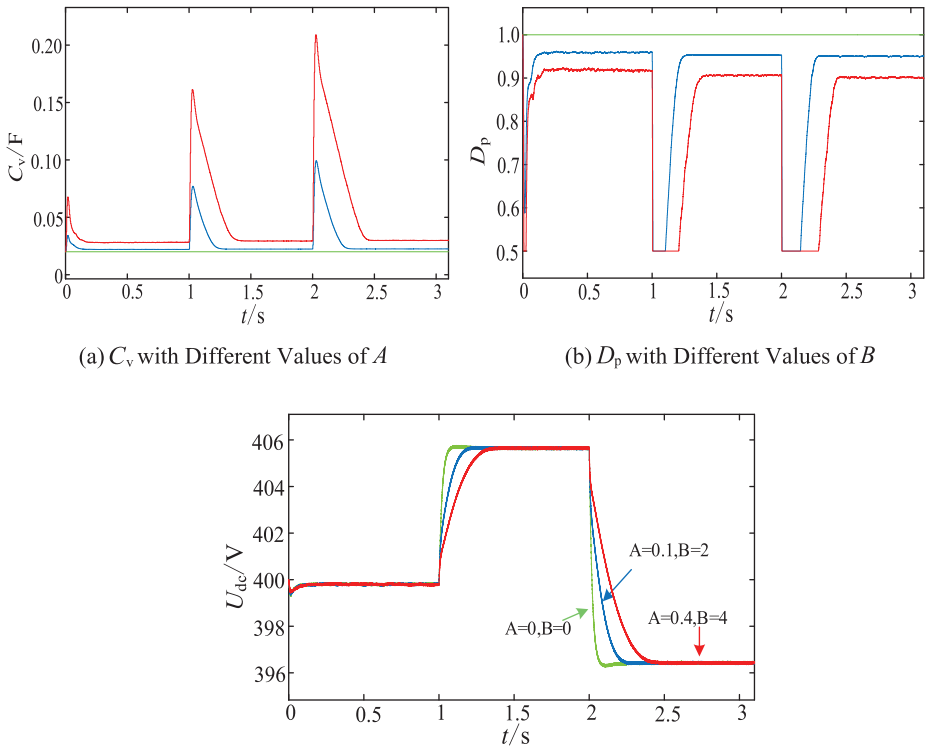

(a) C_v with Different Values of A (b) D_p with Different Values of B

(c) DC Bus Voltage of Different Values of A and B

Figure 14: Simulation waveform of the effects produced by A and B

In Fig. 14c, with the increase of A and B, C_v becomes larger and D_p becomes smaller. By adjusting the values of A and B, the values of C_v and D_p can be modified, enabling the implementation of the AVSG adaptive control. This improvement enables the AVSG controller to detect changes in the DC bus voltage with greater sensitivity.

5 Conclusions

In view of the low inertia and poor anti-interference capability of the DC microgrid equipped with power electronic converters, the AVSG control with virtual capacitance C_v and damping coefficient D_p is applied to the battery interface converter. Furthermore, the adaptive control of C_v and D_p is introduced based on the AVSG control to adapt to changes in the DC bus voltage. Analyzing the simulation results leads to the following conclusions:

(1) By incorporating C_v and D_p with inertial characteristics, the AVSG control mitigates the battery's constrained voltage regulation capacity to some extent and addresses the issue of battery overshooting.

(2) The implementation of the AVSG adaptive control with voltage change rate tracking coefficients A and B enables the attainment of flexible adjustments for C_v and D_p. Properly increasing C_v and decreasing D_p can further enhance the stability of the DC bus voltage, optimize battery performance, and bolster the overall system inertia.

(3) When power step disturbances occur in the microgrid, the AVSG adaptive control can further slow down the dynamic changes in the DC bus voltage and restrain sudden changes in the DC bus voltage. During random power fluctuations, the fluctuation of the DC bus voltage decreases noticeably. In both scenarios, the stability of the DC bus voltage is optimal under adaptive control, and the DC microgrid connected to the DC bus exhibits the characteristics of "flexible inertia".

(4) This study exclusively concentrates on the adaptive control of C_v and D_p for the DC/DC converter within a single energy storage unit in a DC microgrid. The coordinated control of multiple energy storage converters is not taken into account, representing a limitation of this study and a potential avenue for future research.

Acknowledgement: None.

Funding Statement: This work was funded by the National Natural Science Foundation of China (52067013), and the Provincial Natural Science Foundation of Gansu (20JR5RA395).

Author Contributions: The authors confirm their contribution to the paper as follows: Study conception and design: Feng Zhao, Jinshuo Zhang, Xiaoqiang Chen and Ying Wang. Data collection: Feng Zhao, Jinshuo Zhang, Xiaoqiang Chen and Ying Wang. Analysis and interpretation of results: Feng Zhao and Jinshuo Zhang. Draft manuscript preparation: Feng Zhao, Jinshuo Zhang. All authors reviewed the results and approved the final version of the manuscript.

Availability of Data and Materials: Data supporting this study are included within the article.

Conflicts of Interest: The authors declare that they have no conflicts of interest to report regarding the present study.

References

1. Sun, E., Shi, J., Zhang, L., Ji, H., Zhang, Q. et al. (2023). An investigation of battery energy storage aided wind-coal integrated energy system. *Energy Engineering, 120(7),* 1583–1602. https://doi.org/10.32604/ee.2023.027790
2. Deng, X., Da, F., Shao, H., Wang, X. (2023). A survey of the researches on grid-connected solar power generation systems and power forecasting methods based on ground-based cloud Atlas. *Energy Engineering, 120(2),* 385–408. https://doi.org/10.32604/ee.2023.023480
3. Zhang, W. L., Zhang, H., Zhi, N. (2023). Energy management optimization strategy of DC microgrid based on consistency algorithm considering generation economy. *Energy Reports, 9(2),* 683–691. https://doi.org/10.1016/j.egyr.2023.03.060
4. Mansoor, M., Mirza, A. F., Ling, Q., Javed, M. Y. (2020). Novel grass hopper optimization based MPPT of PV systems for complex partial shading conditions. *Solar Energy, 198,* 499–518. https://doi.org/10.1016/j.solener.2020.01.070
5. Rahman, M. S., Hossain, M. J., Lu, J., Pota, H. R. (2018). A need-based distributed coordination strategy for EV storages in a commercial hybrid AC/DC microgrid with an improved interlinking converter control topology. *IEEE Transactions on Energy Conversion, 33(3),* 1372–1383. https://doi.org/10.1109/TEC.2017.2784831
6. Adib, A., Fateh, F., Mirafzal, B. (2021). Smart inverter stability enhancement in weak grids using adaptive virtual-inductance. *IEEE Transactions on Industry Applications, 57(1),* 814–823. https://doi.org/10.1109/TIA.2020.3034070

7. Li, C., Yang, Y., Cao, Y., Aleshina, A., Xu, J. et al. (2023). Grid inertia and damping support enabled by proposed virtual inductance control for grid-forming virtual synchronous generator. *IEEE Transactions on Power Electronics, 38(1),* 294–303. https://doi.org/10.1109/TPEL.2022.3203049
8. Ahmed, M., Meegahapola, L., Vahidnia, A., Datta, M. (2022). Adaptive virtual impedance controller for parallel and radial microgrid with varying X/R ratios. *IEEE Transactions on Sustainable Energy, 13(2),* 830–843. https://doi.org/10.1109/TSTE.2021.3133413
9. Babayomi, O., Li, Y., Zhang, Z. (2022). Distributed consensus-based reactive power sharing in microgrid: A predictive virtual capacitance control technique. *International Journal of Electrical Power and Energy Systems, 141,* 108–139. https://doi.org/10.1016/j.ijepes.2022.108139
10. Samanta, S., Mishra, J. P., Roy, B. K. (2018). Virtual DC machine: An inertia emulation and control technique for a bidirectional DC-DC converter in a DC microgrid. *IET Electric Power Applications, 12(6),* 874–884. https://doi.org/10.1049/iet-epa.2017.0770
11. Liu, Z., Liu, Y. (2022). Virtual DC machine control strategy for stability improvement in DC microgrid with constant power loads. *5th IEEE International Electrical and Energy Conference*, pp. 2893–2899. Nanjing, China. https://doi.org/10.1109/CIEEC54735.2022.9846249
12. He, F. Q., Li, Z. Y., Yang, R. F., Wang, G. L. (2020). Active virtual DC generator technique for new-energy unit of offshore platform. *Ship Engineering, 42(10),* 90–96. https://doi.org/10.13788/j.cnki.cbgc.2020.10.16
13. Tan, S. C., Dong, G., Zhang, H., Zhi, N., Xiao, X. (2016). Virtual DC machine control strategy of energy storage converter in DC microgrid. *2016 IEEE Electrical Power and Energy Conference*, Ottawa, ON, Canada. https://doi.org/10.1109/EPEC.2016.7771749
14. Zhao, F., Xiao, C. R., Chen, X. Q., Wang, Y. (2023). Research on virtual DC generator-based control strategy of DC microgrid with photovoltaic and energy storage. *Energy Engineering, 120(6),* 1353–1370. https://doi.org/10.32604/ee.2023.025976
15. Song, J., Gao, X., Sun, H., Guo, W. (2022). Improved virtual inertia damping adaptive VDG control strategy for DC microgrid hybrid energy storage converter. *4th International Conference on Electrical Engineering and Control Technologies*, pp. 1188–1192. Shanghai, China. https://doi.org/10.1109/CEECT55960.2022.10030597
16. Zhi, N., Ming, X., Ding, Y., Du, L., Zhang, H. (2022). Power-loop-free virtual DC machine control with differential compensation. *IEEE Transactions on Industry Applications, 58(1),* 413–422. https://doi.org/10.1109/TIA.2021.3119512
17. Wang, P., Zhao, J., Liu, K. (2021). Parameter-adaptation-based virtual DC motor control method for energy storage converter. *IEEE Access, 9,* 90795–90804. https://doi.org/10.1109/ACCESS.2021.3091699
18. Cao, J. B., Wang, L., Huang, H., Wu, J. L., Gao, Y. L. et al. (2021). Virtual inertia control strategy of multi-port converter used in DC micro-grid. *Power System Technology, 45(7),* 2604–2615. https://doi.org/10.13335/j.1000-3673.pst.2020.0562
19. Zhu, X. R., Meng, F. Q., Xie, Z. Y. (2019). Control strategy for DC microgrid DC-DC converter based on virtual synchronous generator. *Automation of Electric Power Systems, 43(21),* 132–140. https://kns.cnki.net/kcms/detail/32.1180.TP.20190611.1745.002.html
20. Wu, W. H., Chen, Y. D., Luo, A., Zhou, L. M., Zhou, X. P. (2017). A virtual inertia control strategy for bidirectional grid-connected converters in DC micro-grids. *Proceedings of the CSEE, 37(2),* 360–370 (In Chinese). https://doi.org/10.13334/j.0258-8013.pcsee.161050
21. Cao, X. H., Liu, Y. L., Miao, S. H., Li, L., Liu, Z. W. et al. (2020). Research on virtual inertial control strategy of DC/DC converter in DC microgrid considering self-adaptive parameters. *High Voltage Engineering, 46(4),* 1281–1290. https://doi.org/10.13336/j.1003-6520.hve.20200430020
22. Zeng, G. H., Liao, H. F., Zhao, J. B., Zhu, X. C. (2022). A self-adaptive control strategy of virtual inertia and a damping coefficient for bidirectional DC-DC converters in a DC microgrid. *Power System Protection and Control, 50(6),* 65–73 (In Chinese). https://doi.org/10.19783/j.cnki.pspc.210815